Synthesis of SnO_2 for Thermoelectric Applications Using the Hydrothermal, Co-precipitation, and Co-Precipitation Sonication Methods

Izzatunnisa Azzahra[1*], *Chusnana Insjaf* Yogihati[1], *Alma Nur Roisatul* Masruhah[1,2], *Reza Akbar* Pahlevi[1,2], and *Markus* Diantoro[1,2]

[1]Department of Physics, Faculty of Mathematics, State University of Malang, Jl. Semarang 5, Malang 65145, Indonesia
[2]Center of Advanced Materials for Renewable Energy (CAMRY), State University of Malang, Jl. Semarang 5, Malang 65145, Indonesia

Abstract. Tin oxide (SnO_2) holds promise in thermoelectric applications. The paper explores the preparation of SnO_2 nanoparticles by employing various methods. Synthesis of SnO_2 material is carried out using a comparison of several methods, including the hydrothermal method, co-precipitation method, and co-precipitation sonication. This comparison aims to identify the most efficient method for SnO_2 synthesis with the best performance in thermoelectric applications. Characterization techniques such as SEM-EDX, XRD, and thermoelectric properties, electrical resistivity, electrical conductivity were utilized. Results obtained in the thermoelectric performance test, specifically electrical resistivity and electrical conductivity, showed a decrease in resistivity with increasing temperature for all three methods. In the hydrothermal method, excessively high temperatures led to difficulties in accurately measuring electrical resistivity. The co-precipitation method proved to be the most effective for SnO_2 synthesis.

1 Introduction

Low-grade residual heat energy in the current environment generates approximately 63% (<100°C) [1], [2] leading to climate issues and low energy utilization efficiency [1], [3]–[5]. About two-thirds of this heat energy is dissipated into the environment [6] causing environmental damage and adverse effects on human life, prompting many researchers to conduct studies on renewable energy to address these issues [7]–[9] of this residual heat can be converted into energy [10], [11], thus enabling the development of an environmentally friendly energy system [12], [13]. Alternative energy storage in electronic devices is used in renewable applications [14]–[17]**.** In response to the increasing demand for alternative energy sources, thermoelectric performance [18]–[21] is utilized. Thermoelectricity has become one of the solutions to the current renewable energy crisis [22][23], converting heat energy into electrical energy [6], [24]–[26].

The utilization of waste heat to generate electricity can reduce the harmful environmental impact [27]. Thermoelectric research has increased in the 20th century due to its adaptable nature [28]. Thermoelectricity is a renewable energy source that converts heat into electricity through the Seebeck effect [29]–[33], providing high efficiency [34]–[36] and reducing carbon dioxide emissions 48. Potential thermoelectric materials have electrical conductivity with low thermal conductivity, a large Seebeck coefficient, and dimensionless merit factor efficiency [30], [37], measured by power factor [38]. Thermoelectric materials have become the most environmentally friendly materials [39]. One environmentally friendly thermoelectric material with good thermal and electrical conductivity is SnO_2 [40].

Thermoelectrics have attracted significant attention because they can convert heat energy into electrical energy (Seebeck effect) and convert electrical energy into heat energy (Peltier effect) [41]–[44] The abundance of thermoelectric materials makes it a promising area of research. The performance of thermoelectrics is influenced by three effects: the Seebeck effect, the Peltier effect, and the Thomson effect. The Seebeck effect is a thermoelectric phenomenon that occurs when there is a temperature difference between two different semiconductors, resulting in a voltage difference between them. The Peltier effect involves the presence of a cooler or heater with electrified junctions between two different conductors. Consequently, when current flows, heat is either released or absorbed at these junctions. The Thomson effect relates to the Peltier and Seebeck effects and refers to the heat release or absorption that can be reversed in a homogeneous material. The Thomson effect occurs in a system of a single substance, whereas the Peltier and Seebeck effects require the presence of two different materials since the Seebeck coefficient yields some voltage generated from the temperature difference,

* Corresponding author: markus.diantoro.fmipa@um.ac.id

and the Peltier coefficient yields some heat carried per unit charge [45][46].

Thermoelectrics combine high electrical conductivity with low electronic thermal conductivity. [14], [17]. Electrical conductivity is directly related to electronic thermal conductivity, so high electrical conductivity results in high electronic thermal conductivity [47]. Good thermoelectrics have low thermal conductivity and high electrical conductivity [48]–[50]. Efficiency in thermoelectrics is determined by the Fig of merit (ZT) [51], [52]

$$ZT = S^2\sigma T/K \quad (1)$$

For electrical resistivity determined by the equation

$$\rho = V/I \, . \, A/t \quad (2)$$

Electrical conductivity is determined by the equation

$$\sigma = 1/\rho \quad (3)$$

Tin oxide (SnO_2) is an n-type semiconductor [53] and is one of the fundamental thermoelectric materials [54]. SnO_2 has undergone significant commercialization due to its good thermal and electrical stability [55], [56]. In the crystal structure, SnO_2 has 4 oxygen atoms and 2 tin atoms, with a bandgap energy of approximately ~3.6 eV [57]–[59]. Pure SnO_2 exhibits n-type electrical transport [60]. Many studies have been conducted to synthesize SnO_2 nanostructures using various methods, including spray pyrolysis [61], hydrothermal methods [62], sol-gel methods [63], [64], and co-precipitation. Many of these studies employ various doping methods to improve performance. To determine which method yields good thermoelectric performance, SnO2 synthesis was conducted using three methods: hydrothermal, co-precipitation, and sonication-assisted co-precipitation.

In maximizing the ZT value of a material, several criteria need to be considered as follows: (i) Low thermal conductivity to maintain a temperature difference between two materials. (ii) High electrical conductivity to reduce resistance in the material and produce Joule heating. (iii) High Seebeck coefficient to generate high power [42]. The Seebeck coefficient is a value measured based on the amount of electrical voltage generated from the temperature difference between two sides of a thermoelectric material. The Seebeck coefficient is used to assess the material's ability in thermoelectrics to create a temperature difference with electrical voltage. Measurements in thermoelectric materials depend on how the material can insulate or conduct.

Metal oxide-based materials are considered good candidates for thermoelectrics due to their high ionic properties, abundance in nature, and non-toxic nature [65]. Tin oxide (SnO_2) is a semiconductor material used in thermoelectrics and is of n-type. This thermoelectric material can be experimentally studied over a wide temperature range and is thus widely used in various applications such as lithium-ion batteries [54], sensors, supercapacitors [66], photocatalysts [67] due to its stable physical and chemical properties, high light sensitivity, and excellent electrical characteristics. The thermoelectric performance of SnO_2 is limited by its high thermal conductivity [68], [69] and low intrinsic electrical conductivity. SnO_2 is a widely used thermoelectric material, valued for its excellent properties, including its stability as a metal oxide semiconductor [61], [70]. The porous structure of SnO_2 can enhance its thermoelectric performance compared to a dense structure by adding heavy metals to improve its thermoelectric properties. Its electrical conductivity combined with good thermal stability makes SnO_2 a promising candidate for thermoelectric applications.

In this research, experiments were conducted to synthesize SnO_2 using three different methods to compare which method yields the best thermoelectric performance. This study aimed to determine the crystal structure, morphology, and thermoelectric performance electricity resistivity of SnO_2 materials.

2 Method

2.1. Material and Equipment

In this research, the materials used include $SnCl_2.2H_2O$ (Merck), NaOH (Merck), Etanol, DI Water, and DD water. The equipment used consists of a digital balance, hotplate/stirrer, stainless steel spatula, magnetic stirrer, glass pipette, anatomical forceps, beaker glass, autoclave, oven, centrifuge, vacuum furnace, mortar, alumina crucible, and ultrasonic bath.

2.2. Synthesis of SnO_2 Hydrothermal Method

In a glass beaker, tin chloride dihydrate $SnCl_2.2H_2O$ was dissolved in 90.2 ml of deionized water using a magnetic stirrer and stirred for 40 minutes. In a separate glass beaker, NaOH was dissolved using a magnetic stirrer and stirred for 10 minutes. Then, the NaOH solution was added to the glass beaker with the $SnCl_2.2H_2O$ solution and stirred for 30 minutes at 500 rpm until homogeneous. The mixture was then placed in an autoclave at a temperature of 140°C for 12 hours. After autoclaving, the mixture was centrifuged five times, with each centrifugation lasting for 10 minutes. It was then washed with deionized water and ethanol. The precipitate was then placed in an oven at 80°C for 4 hours. The resulting SnO_2 powder, obtained through the hydrothermal synthesis method, is a yellow powder.

2.3 Synthesis of SnO_2 by Co-Precipitation Method

In a glass beaker, tin chloride dihydrate $SnCl_2.2H_2O$ was dissolved in 56.374 ml of double-distilled water using a magnetic stirrer and stirred for 40 minutes. In a separate glass beaker, NaOH was dissolved using a magnetic stirrer and stirred for 10 minutes. Then, the NaOH solution was added to the glass beaker with the $SnCl_2.2H_2O$ solution and stirred for 2 hours at 500 rpm until homogeneous. The SnO_2 solution was then subjected to centrifugation five times, with each centrifugation lasting for 10 minutes, followed by washing with double-

distilled water and ethanol. The precipitate was then placed in an oven at 80°C for 4 hours and in a furnace at 5000°C for 2 hours. The final result of the SnO_2 synthesis using the co-precipitation method is a white powder.

2.4 Synthesis of SnO_2 by Co-Precipitation Sonication Method

In a glass beaker, tin chloride dihydrate $SnCl_2.2H_2O$ was dissolved in 56.374 ml of double-distilled water using a magnetic stirrer and stirred for 40 minutes. In a separate glass beaker, NaOH was dissolved using a magnetic stirrer and stirred for 10 minutes. After NaOH and $SnCl_2.2H_2O$ were dissolved, they were sonicated for 20 minutes. Then, the NaOH and $SnCl_2.2H_2O$ solutions were mixed and stirred for 2 hours at 500 rpm. The resulting SnO_2 solution was subjected to centrifugation five times, with each centrifugation lasting for 10 minutes, followed by washing with double-distilled water and ethanol. The precipitate was then placed in an oven at 80°C for 4 hours and in a furnace at 5000°C for 2 hours. The final result of the SnO_2 synthesis using the co-precipitation sonication method is a white-colored powder.

3 Results and Discussion

3.1. Nanoparticle Characterization of SnO_2

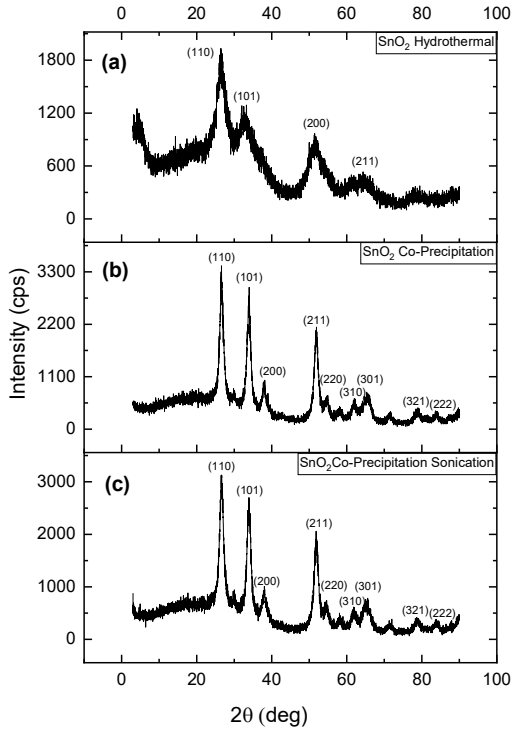

Fig 1. XRD pattern SnO_2 via (a) hydrothermal method, (b) co-precipitation method, and (c) co-precipitation sonication.

The phase composition and crystal structure of all samples were characterized using XRD in the 4° to 80° range for SnO_2, as shown in Fig 1. a using the hydrothermal method. Six diffraction peaks were obtained in this XRD data. The peaks at 26.52°, 32.54°, 51.07°, and 64.2°correspond to (110), (101), (200), and (211). In the XRD of SnO_2, there is a shift in peaks and the loss of several peaks, resulting in significantly different XRD results compared to other studies on SnO_2 according to research by Aminuddin [71]. The shift in peaks and the presence of different peaks suggest the possibility that in the hydrothermal synthesis of SnO_2, it may be necessary to repeat the synthesis and pay attention to the mass of each material during the synthesis of SnO_2. The XRD results obtained for the hydrothermal method of SnO_2 showed the same as research by Pengyu Ren [72], with a total of four identified peaks.

The phase composition and crystal structure of all samples were characterized using XRD, in the range of 4° to 90° for SnO_2, employing the co-precipitation method as depicted in Fig 1b. In this XRD data, nine diffraction peaks were identified. The peaks at 26.56°, 33.93°, 37.815°, 51.91°, 54.75°, 61.99°, 65.70°, 78.75°, and 83.83° correspond to (110), (101), (200), (211), (220), (310), (301), (321), and (222). In the XRD of SnO_2 using the co-precipitation method, the obtained results are consistent with previous research by Aminuddin [71] and research by in the same diffraction Diantoro [73], showing the same 2 theta values and peaks. The co-precipitation method proves to be one of the effective techniques for synthesizing SnO_2.

The phase composition and crystal structure of all samples were characterized using XRD, in the range of 4° to 90° for SnO_2, employing the co-precipitation-sonication method as depicted in Fig 1c. In this XRD data, nine diffraction peaks were identified. The peaks at 26.59°, 33.87°, 37.89°, 51.91°, 54.67°, 61.80°, 65.29°, 78.84°, and 83.89° correspond to (110), (101), (200), (211), (220), (310), (301), (321), and (222). In the XRD of SnO2 using the co-precipitation-sonication method, the obtained results are consistent with previous research by Aminuddin [71], showing the same 2 theta values and peaks. The co-precipitation-sonication method proves to be one of the effective techniques for synthesizing SnO_2, as evidenced by the 2 theta results not differing significantly from the XRD results obtained using the co-precipitation method. The addition of sonication in the synthesis does not make a significant difference in the XRD characterization results compared to the co-precipitation method. However, the addition of the sonication during synthesis resulted in peak shifts observed in the XRD results. This occurred because when sonication was applied, it led to faster reactions, thereby preventing complete nucleation and crystal development, as stated in research by Hala [74].

The observed peaks have agreed with the tetragonal rutile structure and are well-matched with standard values for bulk SnO_2 (JCPDS card no. 41–1445) for co-precipitation method and co-precipitation sonication method at Divya [75].

SEM was used to characterize the surface morphology of nanoparticles, as shown in Fig 2. In the SnO_2 sample synthesized using the hydrothermal method, small spherical shapes were observed, likely influenced by the rapid heating rate during the development phase. The surface morphology exhibits a porous arrangement, and SnO_2 is often employed for doping additions due to the impact of oxygen vacancies on thermoelectric applications in the research of Ashfaq [7].

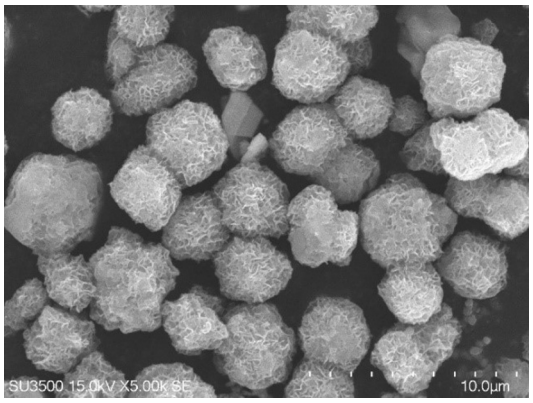

Fig 2. SEM images of SnO_2 via hydrothermal method

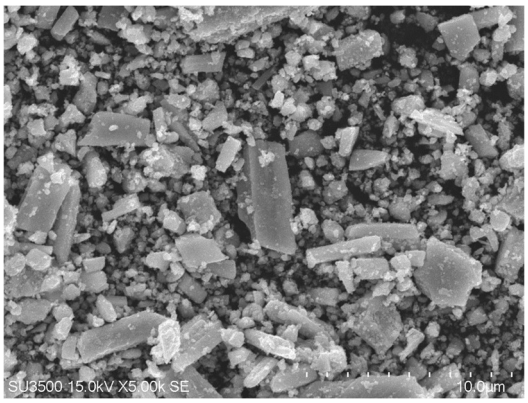

Fig 3. SEM images of SnO_2 via co-precipitation method

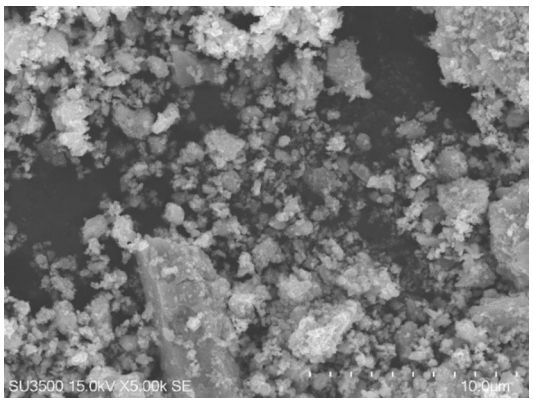

Fig 4. SEM images of SnO_2 via co-precipitation sonication method

Fig 3 depicts the morphology on the surface of SnO_2. In this image, nanoparticles with good crystal properties are observed. The shape of SnO_2 nanoparticles in the co-precipitation method indicates the presence of strong hydrogen bonds during the synthesis process. Therefore, the SEM morphology in the co-precipitation method can be utilized for applications in thermoelectrics in research Divya [75].

The SEM image of SnO_2 nanoparticles using the co-precipitation-sonication method Fig 4 reveals the presence of powder agglomeration. The image shows a clustered morphological structure with homogeneous and uniform agglomeration as in the previous research by Chun Yu [76]. Agglomeration can occur during the synthesis process where unstable temperatures affect the sample's morphology.

3.2. Resistivity and Conductivity Thermoelectric Properties Nanoparticle of SnO_2

To determine the thermoelectric properties of the synthesized samples, we turned the samples into pellet forms (1.00 × 1.00 cm). The thermoelectric properties were conducted by measuring the resistance of the SnO_2 samples while increasing the temperature from 30°C to 100°C. These measurements were performed on each sample using three methods: hydrothermal, co-precipitation, and co-precipitation sonication methods. The results of the electrical resistivity and electrical conductivity are shown in Table 1 and Table 2, accompanied by graphs obtained from each measurement in Fig 5 and Fig 6.

Table 1. Electrical Resistivity of Nanoparticle SnO_2

T (°C)	Hydrothermal	Co-Precipitation	Co-Precipitation Sonication
30	30,8269	29,4218	13,1095
40	29,75935	28,4955	11,61015
50	29,05285	28,67605	11,4296
60	-	28,2286	27,74975
70	-	27,62415	-
80	-	27,15315	-

Fig 5a depicts the electrical resistivity, which is a thermoelectric parameter of the Hydrothermal SnO_2 sample. The results show that as the temperature increases, the resulting resistivity decreases, following the principles of thermoelectricity, where increasing temperature leads to a decrease in electrical resistivity. However, in the synthesis of SnO_2, when the temperature reaches 60°C, the measured electrical resistance increases tenfold, as well as when the temperature reaches 70°C. When the temperature reaches 80°C, the electrical resistance cannot be measured as it reaches a value of 0. This may occur because the material has extremely high resistance, where as it should have a decreasing resistivity with increasing temperature. Therefore, the hydrothermal method used in this study may not be suitable for thermoelectric applications research by Ashfaq [7].

The comparison of electrical resistivity with temperature, a thermoelectric parameter of the Co-Precipitation SnO_2 sample, is shown in Fig 5b. The results indicate that as the temperature increases, the resulting resistivity decreases, aligning with the principles of thermoelectricity, where an increase in temperature leads to a decrease in electrical resistivity. The SnO_2 co-precipitation exhibits relatively good resistivity, as with each temperature increase, the resulting resistivity decreases. At 50 °C, there is a slight increase in resistivity, possibly due to measurement inaccuracies or a room temperature rise. From 60°C to 80°C, the resistivity decreases again. However, at 90°C, there is a significant increase in temperature, which needs further investigation. In this study, the co-precipitation method proves to be the most effective for thermoelectric applications in SnO_2 synthesis as in the preview research by Budi [77] [75].

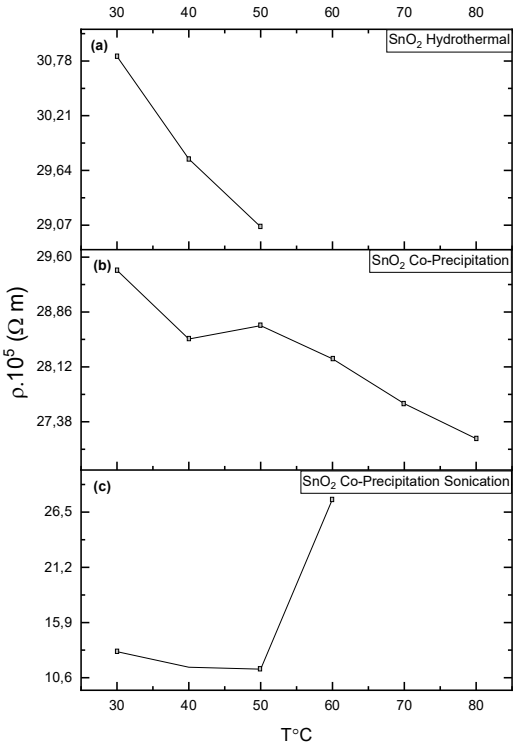

Fig 5. Temperature-dependent electrical resistivity SnO_2 via (a) hydrothermal, (b) co-precipitation, and (c) co-precipitation sonication methods.

The electrical resistivity of SnO_2 using the co-precipitation-sonication method is depicted in Fig 5c. Electrical resistivity is a thermoelectric parameter. The results show that as the temperature increases, the resulting resistivity decreases, following the principles of thermoelectricity where increasing temperature leads to a decrease in electrical resistivity. However, in the synthesis of SnO_2 using the co-precipitation-sonication method, when the temperature reaches 60°C, there is a twofold increase in electrical resistance. Consequently, at 70°C, there is a significant increase, reaching 10 times the resistivity at 60°C. This indicates that the co-precipitation sonication method needs further examination and experimentation to meet thermoelectric.

The electrical resistivity of SnO_2 using the co-precipitation sonication method is depicted in Fig 5c. Electrical resistivity is a thermoelectric parameter. The results show that as the temperature increases, the resulting resistivity decreases, following the principles of thermoelectricity where increasing temperature leads to a decrease in electrical resistivity as in the preview of research by Chafia [78]. However, in the synthesis of SnO_2 using the co-precipitation sonication method, when the temperature reaches 60°C, there is a twofold increase in electrical resistance. Consequently, at 70°C, there is a significant increase, reaching 10 times the resistivity at 60°C. This indicates that the co-precipitation-sonication method needs further examination and experimentation to meet thermoelectric parameters. The measurement of electrical resistivity in the comparison of three methods used in measuring SnO_2 material for thermoelectric properties is presented in Table 1.

Conclusion

Thermoelectricity has emerged as a solution to the current renewable energy crisis, converting heat energy into electrical energy. Thermoelectric materials are considered the most environmentally friendly materials. One such environmentally friendly thermoelectric material with excellent thermal and electrical conductivity is SnO_2. Using three different synthesis methods on SnO_2 yields varying results in thermoelectric utilization. The co-precipitation method, in particular, produces favorable outcomes in terms of XRD, SEM, and electrical resistivity for thermoelectric applications.

References

1 Z. Li, Y. Xu, J. Cui, H. Dou, and X. Zhang, 'High-efficiency zinc thermal charging supercapacitors enabled by hierarchical porous carbon electrodes', *J Power Sources*, vol. 555, Jan. 2023, doi: 10.1016/j.jpowsour.2022.232386.

2 J. Ling-Chin, H. Bao, Z. Ma, W. Taylor, and A. Paul Roskilly, 'State-of-the-Art Technologies on Low-Grade Heat Recovery and Utilization in Industry', in *Energy Conversion - Current Technologies and Future Trends*, IntechOpen, 2019. doi: 10.5772/intechopen.78701.

3 S. Hur *et al.*, 'Low-grade waste heat recovery scenarios: Pyroelectric, thermomagnetic, and thermogalvanic thermal energy harvesting', *Nano Energy*, vol. 114, Sep. 2023, doi: 10.1016/j.nanoen.2023.108596.

4 H. Ma *et al.*, 'Powerful Thermogalvanic Cells Based on a Reversible Hydrogen Electrode and Gas-Containing Electrolytes', *ACS Energy Lett*, vol. 4, no. 8, pp. 1810–1815, Aug. 2019, doi: 10.1021/acsenergylett.9b00944.

5 L. Kush, S. Srivastava, C. Sasikumar, S. K. Vajpai, Y. Srivastava, and Y. Jaiswal, 'Composition-dependent tunability of thermoelectric properties at low temperature for Pr-doped LPFCO double perovskite', *Journal of Materials Science: Materials in Electronics*, vol. 33, no. 22, pp. 17535–17550, Aug. 2022, doi: 10.1007/s10854-022-08616-9.

6 Y. Huang, X. Zhao, J. Le Ke, X. J. Zha, J. Yang, and W. Yang, 'Engineering nanoscale solid networks of ionogel for enhanced thermoelectric power output and excellent mechanical properties', *Chemical Engineering Journal*, vol. 456, Jan. 2023, doi: 10.1016/j.cej.2022.141156.

7 A. Ashfaq *et al.*, 'Enhancing the thermoelectric power factor of nanostructured SnO2 via Bi substitution', *Ceram Int*, vol. 49, no. 7, pp. 10360–10364, Apr. 2023, doi: 10.1016/j.ceramint.2022.11.216.

8 Z. Zhou *et al.*, 'Multiple effects of Bi doping in enhancing the thermoelectric properties of SnTe', *J Mater Chem A Mater*, vol. 4, no. 34, pp. 13171–13175, 2016, doi: 10.1039/c6ta04240f.

9 G. Yang *et al.*, 'Enhanced thermoelectric performance and mechanical strength of n-type BiTeSe materials produced via a composite strategy', *Chemical Engineering Journal*, vol. 428, Jan. 2022, doi 10.1016/j.cej.2021.131205.

10 J. Wang, Y. Qiang Chen, Y. Jun Liu, G. Kang Liu, R. Jie Cai, and J. Wang, 'Experimental investigation of energy storage and reuse of recovered waste heat based on thermoelectric generation', *Appl Therm Eng*, vol. 219, Jan. 2023, doi: 10.1016/j.applthermaleng.2022.119602.

11 Y. Du *et al.*, 'Multi-objective optimization of an innovative power-cooling integrated system based on gas turbine cycle with compressor inlet air pre-cooling, Kalina cycle, and ejector refrigeration cycle', *Energy Convers Manag*, vol. 244, Sep. 2021, doi: 10.1016/j.enconman.2021.114473.

12 R. Zahedi, A. Ahmadi, and R. Dashti, 'Energy, exergy, exergoeconomic and exergoenvironmental analysis and optimization of quadruple combined solar, biogas, SRC and ORC cycles with methane system', *Renewable and Sustainable Energy Reviews*, vol. 150, Oct. 2021, doi: 10.1016/j.rser.2021.111420.

13 U. Sreevidya, V. Shalini, K. K. Bharathi, E. S. Kumar, M. Prakash, and M. Navaneethan, 'Enhancing the thermoelectric performance by defect structures induced in p-type polypyrrole-polyaniline nanocomposite for room-temperature thermoelectric applications', *Journal of Materials Science: Materials in Electronics*, vol. 33, no. 15, pp. 11650–11660, May 2022, doi: 10.1007/s10854-022-08112-0.

14 K. Yang, K. Cho, S. Yang, Y. Park, and S. Kim, 'A laterally designed all-in-one energy device using a thermoelectric generator-coupled micro supercapacitor', *Nano Energy*, vol. 60, pp. 667–672, Jun. 2019, doi 10.1016/j.nanoen.2019.04.016.

15 Z. Liang *et al.*, 'Next-Generation Energy Harvesting and Storage Technologies for Robots Across All Scales', *Advanced Intelligent Systems*, vol. 5, no. 4, Apr. 2023, doi: 10.1002/aisy.202200045.

16 J. D. Phillips, 'Energy Harvesting in Nanosystems: Powering the Next Generation of the Internet of Things', *Frontiers in Nanotechnology*, vol. 3. Frontiers Media S.A., Mar. 12, 2021. doi: 10.3389/fnano.2021.633931.

17 V. Vignesh *et al.*, 'Thermo-chemically functionalized porous featured bio-carbon based asymmetric supercapacitor for new limits of energy storage', *Surfaces and Interfaces*, vol. 35, Dec. 2022, doi: 10.1016/j.surfin.2022.102418.

18 W. H. Chen, P. H. Wu, and Y. L. Lin, 'Performance optimization of thermoelectric generators designed by multi-objective genetic algorithm', *Appl Energy*, vol. 209, pp. 211–223, Jan. 2018, doi: 10.1016/j.apenergy.2017.10.094.

19 W. Yang, W. Zhu, Y. Yang, L. Huang, Y. Shi, and C. Xie, 'Thermoelectric Performance Evaluation and Optimization in a Concentric Annular Thermoelectric Generator under Different Cooling Methods', *Energies (Basel)*, vol. 15, no. 6, Mar. 2022, doi 10.3390/en15062231.

20 X. Hao *et al.*, 'Performance Optimization for PbTe-Based Thermoelectric Materials', *Frontiers in Energy Research*, vol. 9. Frontiers Media S.A., Oct. 20, 2021. doi: 10.3389/fenrg.2021.754532.

21 Z. Bu *et al.*, 'A record thermoelectric efficiency in tellurium-free modules for low-grade waste heat recovery', *Nat Commun*, vol. 13, no. 1, Dec. 2022, doi: 10.1038/s41467-021-27916-y.

22 G. S. Hegde, A. N. Prabhu, R. Y. Huang, and Y. K. Kuo, 'Reduction in thermal conductivity and electrical resistivity of indium and tellurium co-doped bismuth selenide thermoelectric system', *Journal of Materials Science: Materials in Electronics*, vol. 31, no. 22, pp. 19511–19525, Nov. 2020, doi: 10.1007/s10854-020-04383-7.

23 M. Diantoro, S. K. G. Tiana, U. Sa'adah, R. A. Sawitri, C. I. Yogihati, and Sunaryono, 'Bismuth and thermal induced electrical conductivity of high temperature thermoelectric SrTi1-xBixO3 system', in *AIP Conference Proceedings*, American Institute of Physics Inc., Apr. 2020. doi: 10.1063/5.0000992.

24 C. Fu, Y. Sun, and C. Felser, 'Topological thermoelectrics', *APL Materials*, vol. 8, no. 4. American Institute of Physics Inc., Apr. 01, 2020. doi: 10.1063/5.0005481.

25 A. T. T. Pham *et al.*, 'Improved thermoelectric power factor achieved by energy filtering in ZnO: Mg/ZnO hetero-structures', *Thin Solid Films*, vol. 721, Mar. 2021, doi: 10.1016/j.tsf.2021.138537.

26 X. Shi *et al.*, 'Enhanced thermoelectric properties of hydrothermally synthesized n-type Se&Lu-codoped Bi2Te3', *Journal of Advanced Ceramics*, vol. 9, no. 4, pp. 424–431, Aug. 2020, doi: 10.1007/s40145-020-0382-9.

27 H. B. Kang *et al.*, 'Understanding Oxidation Resistance of Half-Heusler Alloys for in-Air High

Temperature Sustainable Thermoelectric Generators', *ACS Appl Mater Interfaces*, vol. 12, no. 32, pp. 36706–36714, Aug. 2020, doi: 10.1021/acsami.0c08413.

28 Y. Muddassir *et al.*, 'Morphology-dependent thermoelectric properties of mixed phases of copper sulfide (Cu2−xS) nanostructures synthesized by hydrothermal method', *Appl Phys A Mater Sci Process*, vol. 127, no. 6, Jun. 2021, doi: 10.1007/s00339-021-04599-2.

29 S. B. Mary, M. Francis, V. G. Sathe, V. Ganesan, and A. L. Rajesh, 'Enhanced thermoelectric property of nanostructured CaMnO3 by sol-gel hydrothermal method', *Physica B Condens Matter*, vol. 575, Dec. 2019, doi: 10.1016/j.physb.2019.411707.

30 U. Rehman *et al.*, 'Improving the thermoelectric performance of hydrothermally synthesized FeS2 nanoparticles by post sulfurization', *Ceram Int*, vol. 46, no. 12, pp. 20496–20499, Aug. 2020, doi: 10.1016/j.ceramint.2020.05.154.

31 R. Cao, Z. Zhu, X. J. Li, X. Hu, and H. Song, 'Enhanced thermoelectric properties of the Lu-doped and CNT-dispersed Bi 2 Te 3 alloy', *Appl Phys A Mater Sci Process*, vol. 125, no. 2, Feb. 2019, doi: 10.1007/s00339-019-2427-x.

32 P. Li, X. Ai, Q. Zhang, S. Gu, L. Wang, and W. Jiang, 'Enhanced thermoelectric performance of hydrothermally synthesized polycrystalline Te-doped SnSe', *Chinese Chemical Letters*, vol. 32, no. 2, pp. 811–815, Feb. 2021, doi: 10.1016/j.cclet.2020.04.046.

33 S. Ma *et al.*, 'Effects of Ni Magnetic Nanoparticles on Thermoelectric Properties of n-Type Bi2Te2.7Se0.3 Materials', *J Electron Mater*, vol. 49, no. 5, pp. 2881–2889, May 2020, doi: 10.1007/s11664-020-07956-8.

34 G. Tan, M. Ohta, and M. G. Kanatzidis, 'Thermoelectric power generation', doi: 10.2307/26759170.

35 A. Ashfaq *et al.*, 'Al doping induced high thermoelectric performance in Cu2ZnSnS4 nanoparticles synthesized by the hydrothermal method', *Ceram Int*, vol. 47, no. 24, pp. 35356–35360, Dec. 2021, doi: 10.1016/j.ceramint.2021.09.078.

36 Z. A. Akbar, J. W. Jeon, and S. Y. Jang, 'Intrinsically self-healable, stretchable thermoelectric materials with a large ionic Seebeck effect', *Energy Environ Sci*, vol. 13, no. 9, pp. 2915–2923, Sep. 2020, doi: 10.1039/c9ee03861b.

37 J. Jacob *et al.*, 'Improved thermoelectric performance of Al and Sn doped ZnO nanoparticles by the engineering of secondary phases', *Ceram Int*, vol. 46, no. 10, pp. 15013–15017, Jul. 2020, doi: 10.1016/j.ceramint.2020.03.031.

38 E. M. M. Ibrahim *et al.*, 'Effect of surfactant concentration on the morphology and thermoelectric power factor of PbTe nanostructures prepared by a hydrothermal route', *Physica E Low Dimens Syst Nanostruct*, vol. 125, Jan. 2021, doi: 10.1016/j.physe.2020.114396.

39 Y. Bai *et al.*, 'Graphene Oxide Embedded in Bi 2 S 3 Nanosheets by Hydrothermal Method to Enhance Thermoelectric Performance'. [Online]. Available: https://ssrn.com/abstract=4169522

40 L. Zhang *et al.*, 'Octahedral SnO 2 /Graphene Composites with Enhanced Gas-Sensing Performance at Room Temperature', *ACS Appl Mater Interfaces*, vol. 11, no. 13, pp. 12958–12967, Apr. 2019, doi: 10.1021/acsami.8b22533.

41 X. Dai, Z. Huang, and F. Zu, 'Enhanced Thermoelectric and Mechanical Properties of n-type Bi2Te2.7Se0.3 Bulk Alloys by Electroless Plating with Cu', *Journal Wuhan University of Technology, Materials Science Edition*, vol. 34, no. 4, pp. 840–844, Aug. 2019, doi 10.1007/s11595-019-2126-7.

42 M. A. Zoui, S. Bentouba, J. G. Stocholm, and M. Bourouis, 'A review on thermoelectric generators: Progress and applications', *Energies*, vol. 13, no. 14. MDPI AG, Jul. 01, 2020. doi: 10.3390/en13143606.

43 X. D. Zhao *et al.*, 'Enhanced thermoelectric performance of tin oxide through antimony doping and introducing pore structures', *J Mater Sci*, vol. 56, no. 3, pp. 2360–2371, Jan. 2021, doi: 10.1007/s10853-020-05291-1.

44 M. A. A. Mohamed, H. M. Ali, E. M. M. Ibrahim, and M. M. Wakkad, 'Optical, Electrical, and Thermoelectric Properties of Hydrothermally Synthesized Bi 2 Te 3 Nanoflakes', *Physica Status Solidi (A) Applications and Materials Science*, vol. 216, no. 7, Apr. 2019, doi: 10.1002/pssa.201800958.

45 Y. E. Putri, S. M. Said, and M. Diantoro, 'Nanoarchitectured titanium complexes for thermal mitigation in thermoelectric materials', *Renewable and Sustainable Energy Reviews*, vol. 101. Elsevier Ltd, pp. 346–360, Mar. 01, 2019. doi: 10.1016/j.rser.2018.10.006.

46 X. D. Zhao *et al.*, 'Enhanced thermoelectric performance of tin oxide through antimony doping and introducing pore structures', *J Mater Sci*, vol. 56, no. 3, pp. 2360–2371, Jan. 2021, doi: 10.1007/s10853-020-05291-1.

47 X. Dai, J. Nan, and Q. Cheng, 'Enhanced Thermoelectric and Mechanical Properties of p-type Bi0.5Sb1.5Te3 Bulk Alloys by Composite Electroless Plating with Ni&Cu', *Journal Wuhan University of Technology, Materials Science Edition*, vol. 37, no. 5, pp. 1009–1013, Oct. 2022, doi: 10.1007/s11595-022-2624-x.

48 M. Diantoro *et al.*, 'Rapid Preparation of Co1-xMxSb3 (M = Fe, Mn) Skutterudites two series lling: Enabling high-e thermoelectric Rapid Preparation of Co 1-x M x Sb 3 (M = Fe, Mn) Skutterudites two series filling: Enabling high-efficiency thermoelectric', 2023, doi: 10.21203/rs.3.rs-3307402/v1.

49 D. Aditya, A. Sawitri, and M. Diantoro, 'Electrical Properties of Tetrahedrite CuS based Thermoelectric Material', 2018. [Online]. Available: www.sciencedirect.com

50 D. Aditya *et al.*, 'The effect of Ag on the thermoelectric performance of Cu1-xAgxS tetrahedrite/Al prepared using modified polyol methods', in *Journal of Physics: Conference Series*, Institute of Physics Publishing, Jul. 2020. doi: 10.1088/1742-6596/1572/1/012071.

51 Z. R. Yang and C. J. Liu, 'Thermoelectric Transport in p-Type (Pb0.98Na0.02Te)1−x(Zn0.85Al0.15Te)x-Te Composites Fabricated Using a Combination of Hydrothermal Synthesis and Evacuating-and-Encapsulating Sintering', *J Electron Mater*, vol. 49, no. 5, pp. 2954–2961, May 2020, doi: 10.1007/s11664-020-07994-2.

52 F. Wu and W. Wang, 'Thermoelectric Performance of n-Type Polycrystalline Bi2Te3 by Melt Spinning Following High-Pressure Sintering', *J Electron Mater*, vol. 52, no. 1, pp. 276–283, Jan. 2023, doi: 10.1007/s11664-022-09985-x.

53 P. Kumar, S. Kumar, A. Kumar, and V. Verma, 'Lithium-doped SnO2 porous ceramics-based hydroelectric cells: a novel green energy source for sustainable power generation', *Journal of Materials Science: Materials in Electronics*, vol. 32, no. 11, pp. 14833–14845, Jun. 2021, doi: 10.1007/s10854-021-06037-8.

54 L. Chu *et al.*, 'Doping induced enhanced photocatalytic performance of SnO2:Bi3+ quantum dots toward organic pollutants', *Colloids Surf A Physicochem Eng Asp*, vol. 589, Feb. 2020, doi: 10.1016/j.colsurfa.2020.124416.

55 D. G. Pacheco-Salazar, F. F. H. Aragón, L. Villegas-Lelovsky, A. Ortiz de Zevallos, G. E. Marques, and J. A. H. Coaquira, 'Engineering of the band gap induced by Ce surface enrichment in Ce-doped SnO2 nanocrystals', *Appl Surf Sci*, vol. 527, Oct. 2020, doi: 10.1016/j.apsusc.2020.146794.

56 R. G. Drabeski *et al.*, 'Raman and photoacoustic spectroscopies of SnO2 thin films deposited by spin coating technique', *Vib Spectrosc*, vol. 109, Jul. 2020, doi: 10.1016/j.vibspec.2020.103094.

57 M. Kandasamy *et al.*, 'Ni-Doped SnO2 Nanoparticles for Sensing and Photocatalysis', *ACS Appl Nano Mater*, vol. 1, no. 10, pp. 5823–5836, Oct. 2018, doi: 10.1021/acsanm.8b01473.

58 H. Sharma Akkera *et al.*, 'Studies of the effect of Bi-doped on structural, electrical, optical properties of spin-coated SnO2 transparent conducting oxide thin films'. [Online]. Available: https://ssrn.com/abstract=4017500

59 M. P. Subramaniam *et al.*, 'Electrospun SnO2 and its composite V2O5 nanofibers for thermoelectric power generator', *J Solgel Sci Technol*, vol. 98, no. 1, pp. 183–192, Apr. 2021, doi: 10.1007/s10971-020-05443-4.

60 K. Chaibi, M. Benhaliliba, and A. Ayeshamariam, 'Computational assessment and experimental study of optical and thermoelectric properties of rutile SnO2 semiconductor', *Superlattices Microstruct*, vol. 155, Jul. 2021, doi: 10.1016/j.spmi.2021.106923.

61 P. Leangtanom, A. Wisitsoraat, K. Jaruwongrungsee, N. Chanlek, S. Phanichphant, and V. Kruefu, 'Highly sensitive and selective ethylene gas sensors based on CeOx-SnO2 nanocomposites prepared by a Co-precipitation method', *Mater Chem Phys*, vol. 254, Nov. 2020, doi: 10.1016/j.matchemphys.2020.123540.

62 J. Divya, A. Pramothkumar, S. Joshua Gnanamuthu, D. C. Bernice Victoria, and P. C. Jobe prabakar, 'Structural, optical, electrical and magnetic properties of Cu and Ni doped SnO2 nanoparticles prepared via Co-precipitation approach', *Physica B Condens Matter*, vol. 588, Jul. 2020, doi: 10.1016/j.physb.2020.412169.

63 K. Sathiyamurthy, 'Synthesis of pure SnO2 nanospheres by co-precipitation method', *Malaya Journal of Matematik*, vol. S, no. 2, 1247, doi: 10.26637/MJM0S20/0330.

64 D. Maharana, J. Niu, D. Gao, Z. Xu, and J. Shi, ' Electrochemical Degradation of Rhodamine B over Ti/SnO 2 -Sb Electrode ', *Water Environment Research*, vol. 87, no. 4, pp. 304–311, Apr. 2015, doi: 10.2175/106143015x14212658613514.

65 N. L. Kartika *et al.*, 'Thermopower Enhancement of Rutile-type SnO2 Nanocrystalline Using Facile Co-Precipitation Method', *Jurnal Elektronika dan Telekomunikasi*, vol. 20, no. 2, p. 82, Dec. 2020, doi: 10.14203/jet.v20.82-88.

66 Y. C. Chang and S. H. Wu, 'Bi-functional Al-doped ZnO@SnO 2 heteronanowires as efficient substrates for improving photocatalytic and SERS performance', *Journal of Industrial and Engineering Chemistry*, vol. 76, pp. 333–343, Aug. 2019, doi: 10.1016/j.jiec.2019.03.058.

67 N. Rani, K. Khurana, and N. Jaggi, 'Structural and electrical properties of MWCNTs/ SnO2 nanocomposites via hydrothermal and co-precipitation route: A comparative study', *Applied Nanoscience (Switzerland)*, vol. 11, no. 8, pp. 2291–2301, Aug. 2021, doi: 10.1007/s13204-021-01968-4.

68 S. Asaithambi *et al.*, 'Preparation of Fe-SnO2@CeO2 nanocomposite electrode for asymmetric supercapacitor device performance analysis', *J Energy Storage*, vol. 36, Apr. 2021, doi: 10.1016/j.est.2021.102402.

69 J. L. A. Do Nascimento, L. Chantelle, I. M. G. Dos Santos, A. L. M. de Oliveira, and M. C. F. Alves, 'The Influence of Synthesis Methods and Experimental Conditions on the Photocatalytic Properties of SnO2: A Review', *Catalysts*, vol. 12, no. 4. MDPI, Apr. 01, 2022. doi: 10.3390/catal12040428.

70 A. Kumar, M. Chitkara, G. Dhillon, and N. Kumar, ' Facile Synthesis and Structural, Microstructural, and Dielectric Characteristics of SnO 2 -CeO 2 Semiconducting Binary Nanocomposite ', *ECS Trans*, vol. 107, no. 1, pp. 3739–3747, Apr. 2022, doi: 10.1149/10701.3739ecst.

71 A. Debataraja, D. W. Zulhendri, B. Yuliarto, Nugraha, Hiskia, and B. Sunendar, 'Investigation of Nanostructured SnO2 Synthesized with Polyol

Technique for CO Gas Sensor Applications', in *Procedia Engineering*, Elsevier Ltd, 2017, pp. 60–64. doi: 10.1016/j.proeng.2017.03.011.

72 P. Ren, L. Qi, K. You, and Q. Shi, 'Hydrothermal Synthesis of Hierarchical SnO2 Nanostructures for Improved Formaldehyde Gas Sensing', *Nanomaterials*, vol. 12, no. 2, Jan. 2022, doi: 10.3390/nano12020228.

73 M. Diantoro, Kholid, A. A. Mustikasari, and Yudiyanto, 'The Influence of SnO2 Nanoparticles on Electrical Conductivity, and Transmittance of PANI-SnO2 Films', in *IOP Conference Series: Materials Science and Engineering*, Institute of Physics Publishing, Jun. 2018. doi: 10.1088/1757-899X/367/1/012034.

74 F. Aziz *et al.*, 'Facile synthesis of NiO/ZnO nano-composite by Co-precipitation, characterization and photocatalytic study of colored and colorless organic pollutants by solar irradiation', *Physica B Condens Matter*, vol. 640, Sep. 2022, doi: 10.1016/j.physb.2022.413858.

75 J. Divya, A. Pramothkumar, S. Joshua Gnanamuthu, D. C. Bernice Victoria, and P. C. Jobe Prabakar, 'Structural, optical, electrical and magnetic properties of Cu and Ni doped SnO2 nanoparticles prepared via Co-precipitation approach', *Physica B Condens Matter*, vol. 588, Jul. 2020, doi: 10.1016/j.physb.2020.412169.

76 C. Y. Li *et al.*, 'Thermoelectric and mechanical properties of Bi0.42Sb1.58Te3/SnO2 bulk composites with controllable ZT peak for power generation', *J Eur Ceram Soc*, 2023, doi: 10.1016/j.jeurceramsoc.2023.09.082.

77 B. Adiperdana, N. L. Kartika, and I. A. Dharmawan, 'Electronic and Thermoelectric Properties on Rutile SnO2 Under Compressive and Tensile Strains Engineering', *Jurnal Elektronika dan Telekomunikasi*, vol. 22, no. 2, p. 95, Dec. 2022, doi: 10.55981/jet.506.

78 C. Khelifi, A. Attaf, H. Saidi, A. Yahia, and M. Dahnoun, 'Investigation of F doped SnO 2 thin films properties deposited via ultrasonic spray technique for several applications', *Surfaces and Interfaces*, vol. 15, pp. 244–249, Jun. 2019, doi: 10.1016/j.surfin.2019.04.001.